A study of gold nanoparticle blood flow in stenotic arteries with Arrhenius energy and variable viscosity

Kumar Sumit[1,2]* and Kumar Surendra[2]
1. Government College for Women, Gurawara, Rewari, 123035, Haryana, INDIA
2. University Institute of Engineering and Technology, Maharshi Dayanand University, Rohtak, 124001, Haryana, INDIA
*sumit96105@gmail.com

Abstract
This study aims to explore the flow characteristic of a nanofluid $(Au/Blood)$ *containing gyrotactic microorganisms flow through an artery exhibiting mild stenosis. This study finding provide significant insights into the interaction with magnetic field parameter, temperature-dependent viscosity, viscous dissipation, Arrhenius energy, heat source parameter and the nanofluid. The governing flow equations are converted into the dimensionless form using the appropriate similarity transformations. The resulting partial differential equations are subjected to numerical investigation employing the explicit FTCS (forward time central space) numerical technique within the computational framework of MATLAB.*

The major findings are that the increment in the thermal Grashof number leads to rise in the velocity and volumetric flow rate. The increment in the Rayleigh number leads to decline in the velocity profile. The results demonstrate that an increase in the activation energy parameter reduces the Sherwood number and enhances the concentration profile. The current effort holds promise for the advancement of biomedical device design. It offers valuable insights into hemodynamic flow, applied therapeutically within the biomedical sciences.

Keywords: Gold nanoparticles, stenotic artery, Arrhenius energy, variable viscosity, microorganisms.

Introduction

Stenosis is a condition where blood vessels narrow, particularly arteries, leading to impaired blood flow to vital tissues and organs. It is primarily caused by atherosclerosis, where plaque accumulates along the vessel walls, causing serious health complications like heart attacks and strokes. The process begins with endothelial cells damage, often induced by factors like hypertension, smoking and high cholesterol. This damage allows low-density lipoprotein cholesterol to penetrate the endothelium, triggering an immune response. As the condition progresses, a fibrous cap is formed over these deposits, which can thicken and constrict the vessel. In advanced stages, calcification occurs, hardening the plaque and diminishing arterial elasticity. If the fibrous cap ruptures, it could lead to thrombosis, obstructing the artery and causing acute medical crises. The severity of stenosis depends on the degree of narrowing and its anatomical location, with coronary arteries being particularly vulnerable. Understanding these mechanisms is crucial for developing effective prevention and treatment strategies in cardiovascular health[10,16,17,32,34,35]. The gold nanoparticles $(AuNPs)$, ranging from 1 to 100 nano-meters, possess distinctive properties that render them highly advantageous in biomedical fields, particularly concerning blood and arterial health. Their biocompatibility facilitates safe interactions with blood components, allowing for functionalization with biomolecules aimed at targeting specific sites, such as arterial walls, without provoking immune responses[6].

In the realm of drug delivery, $AuNPs$ effectively transport therapeutic agents to diseased regions like atherosclerotic plaques, thereby enhancing treatment efficacy while reducing side effects. They also show potential in improving blood flow dynamics in stenotic arteries by mitigating oxidative stress, dissolving clots and employing photothermal effects to disrupt plaques. Additionally, $AuNPs$ function as efficient contrast agents in medical imaging, improving the visualization of blood flow and arterial blockages due to their optical characteristics. In photothermal therapy, they selectively heat targeted arterial areas to restore blood flow.

In recent decades, researchers have demonstrated great interest in examining the impact of magnetic fields on biological fluids. This curiosity stems from individuals' exposure to magnetic fields of differing intensity in daily life. Magnetic fields have been adeptly employed to direct medicine administration and to control the dynamics and flow of biofluids, including blood. They are essential in the treatment of stenotic arteries by improving medication delivery to the impacted regions. Magnetic nanoparticles encapsulated with pharmaceuticals can be guided to stenotic locations utilizing external magnetic fields. Moreover, magnetic fields can apply stresses on red blood cells within stenotic arteries, generating shear stress that aids in the prevention of blood clot formation.

An early study in this subject was performed by Issacci et al[13], who quantitatively examined the phenomenon of induced magnetic fields in a curved pipe. Employing a toroidal coordinate system, they formulated a solution as a power series applicable to situations with low to moderate Hartmann numbers.

Their findings indicated that augmenting the magnetic field intensity amplifies the fluid-pressure interaction with the tube wall as seen by the observed velocity patterns.

Sajid et al[25] performed a computational analysis examining blood flow dynamics in stenosed arteries incorporating tetra-hybrid nanoparticles. The research demonstrated a notable reduction in blood temperature with the application of tetra-hybrid nanoparticles, indicating superior thermal regulation relative to conventional bi-hybrid and tri-hybrid nanoparticles. In the same direction, Karmakar et al[14] explored the electroosmotic pumping mechanism driven by cilia in blood infused with tetra-hybrid nanoparticles, traversing an eccentrically angled arterial pathway. Their findings demonstrated significant effects on hemodynamic parameters and profiles, especially in response to endoscopic interventions.

Bhatti et al[7] investigated the dynamics of peristaltic motion in a Jeffrey nanofluid, considering the influence of microorganisms and a varying magnetic field. Their research concentrated on elucidating the synergistic impacts of peristalsis and bioconvection within a nanofluid subjected to magnetic fluctuations. In a similar vein, Alharbi et al[4] examined the bioconvection dynamics of microorganisms in a hybrid nanofluid traversing a porous stretching sheet. Their investigation elucidated the interplay between bioconvection and hybrid nanofluids, revealing its impact on fluid dynamics and thermal transfer properties.

A study conducted by Manchi and Ponalagusamy[21] has elucidated multiple facets of $AuNPs$' functions in drug delivery systems, cancer therapy and their influence on blood flow dynamics in arteries affected by stenosis. These studies highlight the promising capabilities of $AuNPs$ in enhancing medical therapies and diagnostic methodologies. Sharma et al[29] investigated pulsatile blood flow within an axisymmetric stenosed artery undergoing axial direction, with a focus on the dependency of blood viscosity on hematocrit concentration.

The periodic pressure gradient resulting from the heart's concentration and relaxation is articulated mathematically via a Fourier series. Their analysis delves into the effects of stenosis thickness and hematocrit concentration on various hemodynamic indicators, showcasing the results through graphical representations to elucidate the complex interrelationship among these variables and the dynamics of blood flow. Priyadharsini and Sheremet[23] performed a numerical simulation to investigate the bioconvective flow of magnetized blood affected by chemical reactions in a preamble artery. Their investigation demonstrated that the heat transfer rate markedly increases when the permeability parameter is minimized, underscoring the essential influence of arterial permeability on regulating heat transfer in magnetized blood flow within bioconvective conditions.

Bioconvection represents an intriguing phenomenon linked to the motility of microorganisms, leading to the generation of convective fluid flow due to density fluctuations arising from hydrodynamic kinetic energy. This concept, first examined in Kuznetsov's[20] foundational research, is crucial in numerous natural and industrial phenomena. Bioconvection is a phenomenon that occurs as a result of the coordinated motion of microorganisms including bacteria and algae, which respond to various stimuli such as light, gradients in oxygen concentration, centrifugal forces, or magnetic fields. The arrangement of these microorganisms in structured patterns within fundamental fluids facilitates the application of bioconvection across various domains.

Illustrative instances encompass biomedical applications such as bio-microsystems, pharmaceutical production, biodegradable polymer synthesis and biosensor technology. Kuznetsov[19] advanced this comprehension by exploring the utilization of nanofluids containing oxytactic microorganisms, highlighting how the interplay between nanoparticles and microbes improves the fluid's dynamic and thermal characteristics. The amalgamation of nanotechnology and bioconvection presents novel opportunities for advancements across medical, environmental and energy sectors. The examination of hemodynamics within arterial structures presents substantial implications for both engineering disciplines and medical practices.

The design of cardiovascular devices and the management of arterial stenosis are fundamentally important, as arterial stenosis significantly contributes to the prevalence of cardiovascular diseases. Clinical research underscores that disruptions in hemodynamics, especially within circulatory regions, play a significant role in the onset and advancement of cardiovascular diseases. Tang et al[31] examined the circulatory dynamics of an Au −nanofluid in stenotic arteries situated within a porous medium, employing the Sisko model while considering the effects of viscous dissipation. The investigation demonstrated that an elevation in the curvature parameter resulted in a decline in the Nusselt number, signifying diminished heat transfer efficiency, concurrently leading to an augmentation in drag force.

Tang et al[30] conducted a numerical analysis of the flow and heat transfer properties of a magnetized gold-blood Oldroyd-B nanofluid within small stenotic arteries. The results indicated that with an increase in flow parameters, there was a corresponding decrease in the Nusselt number, while the drag force exerted on the arterial walls increased. The findings elucidate the significant impact of nanofluids and magnetic phenomena on hemodynamic performance, presenting essential guidance for innovations in the medical and engineering fields aimed at addressing arterial diseases.

The studies referenced indicate notable gaps in our comprehension of the dynamics of Au/blood nanofluids that are infused with gyrotactic microorganisms. The dynamics of nanofluid movement through stenosed arteries, particularly in relation to electroosmotic influences, has not been thoroughly investigated. Addressing this gap is crucial for achieving a thorough comprehension of the flow dynamics, thermal behavior and biological interactions

present in intricate vascular conditions. Expanding on previous studies, our current research examines the dynamics of nanofluids within arteries exhibiting mild stenosis. This research presents a mathematical framework to analyze blood flow that incorporates suspended $AuNPs$ alongside gyrotactic microorganisms and electroosmotic forces.

The governing equations undergo a transformation into a non-dimensional format and are subsequently solved through numerical methods utilizing the FTCS scheme. The outcomes are scrutinized to assess the influence of multiple profiles such as velocity, temperature, nanoparticle concentration, microorganisms' distribution, flow rate, Nusselt number, Sherwood number and wall shear stress (WSS). The results are depicted through comprehensive graphs, offering a deeper understanding of the complex dynamics present in the arterial system.

The objectives of the present study are:

- To examine the effect of nanofluid $(Au/Blood)$ flow containing gyrotactic microorganisms in a stenosed artery.
- To analyse the blood flow properties considering the simultaneous influences of Joule heating, electroosmosis, thermal sources and viscous dissipation.
- To examine the bioconvective blood flow with the effects of Arrhenius energy.

Material and Methods

In this study, we consider the analysis of a laminar, fully developed and incompressible two-dimensional magnetohydrodynamics blood flow in the stenosed artery. The arterial system being examined consists of straight, round cylinders positioned along the artery's centreline, displaying an elliptical configuration of the stenosis within the artery. The study investigates the incompressibility of human blood, including the presence of $AuNPs$ in small arteries. The study examines the flow properties of blood enhanced with $AuNPs$ within a circular region characterized by a radius designated $\bar{r}_1$. The $\bar{z}_1$-axis denotes the direction of blood flow whereas the $\bar{r}_1$-axis is the perpendicular to the $\bar{z}_1$-axis. The mobility of blood is caused by the pulsatile flow generated by the beating of the heart and the antisymmetric, indicating that all variables are independent of $\bar{\theta}_1$. An electric field E_1 is $(0, 0, E_z)$ and a uniform magnetic field B is $(B_r, 0, 0)$. The shape of the arterial elliptical stenosis[17,18] is delineated (Fig. 1) as follows:

$$\bar{R}(\bar{z}_1) = \begin{cases} \bar{R}_0 - \bar{\delta}_s sin\left(\frac{\pi(\bar{z}_1 - \bar{d}_1)}{\bar{L}_1}\right) ; \ \bar{d}_1 \le \bar{z}_1 \le \bar{d}_1 + \bar{L}_1 \\ \bar{R}_0 \qquad\qquad\qquad\qquad ; \quad otherwise \end{cases} \quad (1)$$

where the term $\bar{R}_0$ denoted the radius of the normal artery, $\bar{\delta}_s$ indicated the maximum depth of the stenosis, $\bar{d}_1$ delineated the starting location of the stenosis and finally $\bar{L}_1$ denoted the length of the stenosed part along the $\bar{z}_1$-axis.

The blood flow velocity is $V = \left(\bar{u}_1(\bar{r}_1, \bar{\theta}_1, \bar{z}_1), \bar{v}_1(\bar{r}_1, \bar{\theta}_1, \bar{z}_1), \bar{w}_1(\bar{r}_1, \bar{\theta}_1, \bar{z}_1)\right)$ and the flow is characterized by the following governing equations[2,4,11,16,17,19,26]:

Continuity equation

$$\frac{\partial \bar{u}_1}{\partial \bar{r}_1} + \frac{\bar{u}_1}{\bar{r}_1} + \frac{\partial \bar{w}_1}{\partial \bar{z}_1} = 0 \quad (2)$$

Momentum equation

$\bar{r}_1$-direction

$$\rho_{nf}\left(\frac{\partial \bar{u}_1}{\partial \bar{t}_1} + \bar{u}_1\frac{\partial \bar{u}_1}{\partial \bar{r}_1} + \bar{w}_1\frac{\partial \bar{u}_1}{\partial \bar{z}_1}\right) = -\frac{\partial \bar{p}_1}{\partial \bar{r}_1} + \frac{1}{\bar{r}_1}\frac{\partial}{\partial \bar{r}_1}\left(\mu_{nf}(\bar{T})\bar{r}_1\frac{\partial \bar{u}_1}{\partial \bar{r}_1}\right) + \frac{1}{2}\frac{\partial}{\partial \bar{z}_1}\left(\mu_{nf}(\bar{T})\left(\frac{\partial \bar{w}_1}{\partial \bar{r}_1} + \frac{\partial \bar{u}_1}{\partial \bar{z}_1}\right)\right) - \mu_{nf}(\bar{T})\frac{\bar{u}_1}{\bar{r}_1{}^2} \quad (3)$$

$\bar{z}_1$-direction

$$\rho_{nf}\left(\frac{\partial \bar{w}_1}{\partial \bar{t}_1} + \bar{u}_1\frac{\partial \bar{w}_1}{\partial \bar{r}_1} + \bar{w}_1\frac{\partial \bar{w}_1}{\partial \bar{z}_1}\right) = -\frac{\partial \bar{p}_1}{\partial \bar{z}_1} + \frac{1}{2\,\bar{r}_1}\frac{\partial}{\partial \bar{r}_1}\left(\mu_{nf}(\bar{T})\bar{r}_1\left(\frac{\partial \bar{w}_1}{\partial \bar{r}_1} + \frac{\partial \bar{u}_1}{\partial \bar{z}_1}\right)\right) + \frac{\partial}{\partial \bar{z}_1}\left(\mu_{nf}(\bar{T})\frac{\partial \bar{w}_1}{\partial \bar{z}_1}\right) + (\rho\gamma)_{nf}g(\bar{T} - \bar{T}_1) + (\rho\gamma)_{nf}g(\bar{C} - \bar{C}_1) - (\rho\gamma)_{nf}g(\bar{N} - \bar{N}_1) + G(\bar{t}_1) + \rho_e E_z - \sigma_{nf}B_r^2\bar{w}_1 \quad (4)$$

Energy equation

$$\left(\rho c_p\right)_{nf}\left(\frac{\partial \bar{T}}{\partial \bar{t}_1} + \bar{u}_1\frac{\partial \bar{T}}{\partial \bar{r}_1} + \bar{w}_1\frac{\partial \bar{T}}{\partial \bar{z}_1}\right) = k_{nf}\left(\frac{\partial^2 \bar{T}}{\partial \bar{r}_1{}^2} + \frac{1}{\bar{r}_1}\frac{\partial \bar{T}}{\partial \bar{r}_1} + \frac{\partial^2 \bar{T}}{\partial \bar{z}_1{}^2}\right) + Q + \sigma_{nf}B_r^2\bar{w}_1{}^2 + \sigma_{nf}E_z^2 + 2\mu_{nf}(\bar{T})\left[\left(\frac{\partial \bar{u}_1}{\partial \bar{r}_1}\right)^2 + \left(\frac{\bar{u}_1}{\bar{r}_1}\right)^2 + \left(\frac{\partial \bar{w}_1}{\partial \bar{z}_1}\right)^2 + \frac{1}{2}\left(\frac{\partial \bar{u}_1}{\partial \bar{z}_1} + \frac{\partial \bar{w}_1}{\partial \bar{r}_1}\right)^2\right] \quad (5)$$

Concentration equation

$$\frac{\partial \bar{C}}{\partial \bar{t}_1} + \bar{u}_1\frac{\partial \bar{C}}{\partial \bar{r}_1} + \bar{w}_1\frac{\partial \bar{C}}{\partial \bar{z}_1} = D_c\left(\frac{\partial^2 \bar{C}}{\partial \bar{r}_1{}^2} + \frac{1}{\bar{r}_1}\frac{\partial \bar{C}}{\partial \bar{r}_1} + \frac{\partial^2 \bar{C}}{\partial \bar{z}_1{}^2}\right) - k_r^2\left(\frac{\bar{T}}{\bar{T}_1}\right)^2 exp\left(-\frac{E_b}{k_0\bar{T}}\right)(\bar{C} - \bar{C}_1) \quad (6)$$

Microorganisms equation

$$\frac{\partial \bar{N}}{\partial \bar{t}_1} + \bar{u}_1\frac{\partial \bar{N}}{\partial \bar{r}_1} + \bar{w}_1\frac{\partial \bar{N}}{\partial \bar{z}_1} = D_m\left(\frac{\partial^2 \bar{N}}{\partial \bar{r}_1{}^2} + \frac{1}{\bar{r}_1}\frac{\partial \bar{N}}{\partial \bar{r}_1} + \frac{\partial^2 \bar{N}}{\partial \bar{z}_1{}^2}\right) - \frac{bW_c}{\bar{C}_w - \bar{C}_1}\left(\frac{\partial}{\partial \bar{r}_1}\left(\bar{N}\frac{\partial \bar{C}}{\partial\, \bar{r}_1}\right) + \frac{\partial}{\partial \bar{z}_1}\left(\bar{N}\frac{\partial \bar{C}}{\partial\, \bar{z}_1}\right)\right) \quad (7)$$

Here, $(\bar{u}_1, \bar{v}_1, \bar{w}_1)$ are the components of velocity in growing $(\bar{r}_1, \bar{\theta}_1, \bar{z}_1)$ directions respectively, additionally due to using the antisymmetric condition, neglecting the velocity $\bar{v}_1$ along the direction $\bar{\theta}_1$. The terms E_b, ρ_{nf}, $\mu_{nf}(\bar{T})$, k_0, $-\frac{\partial \bar{p}_1}{\partial \bar{z}_1}$, γ_{nf}, g, $G(\bar{t}_1)$, ρ_e, E_z, σ_{nf}, B_r, $\left(c_p\right)_{nf}$, Q, D_c, k_r, D_m,

$W_c, b, \bar{C}_w, \bar{C}, \bar{C}_1, \bar{N}_w, \bar{N}, \bar{N}_1, \bar{T}_w, \bar{T}, \bar{T}_1$ using in continuity, momentum, energy, concentration and microorganisms equations are indicated as the energy of activation, nanofluid density, nanofluid viscosity, Boltzmann constant, pressure gradient, nanofluid thermal expansion coefficient, acceleration due to gravity, body acceleration, electrical charge density, electrical field, nanofluid electrical conductivity, uniform magnetic field, nanofluid heat capacitance, constant heat absorption or heat generation parameter, diffusivity of the concentration, chemical reaction, diffusivity of the microorganisms, highest acceleration at which a cell may swim, chemotaxis factor, the concentration at the wall, concentration, reference concentration, microorganisms at the wall, microorganisms, reference microorganisms, temperature at the wall, temperature, reference temperature respectively.

Furthermore, the complete expression of the $k_r^2\left(\frac{\bar{T}}{\bar{T}_1}\right)^2 exp\left(-\frac{E_b}{k_0\bar{T}}\right)$ in equation (6) is designated as the revised Arrhenius equation. The boundary conditions are defined according to the aforementioned fluid-flow model from the equations (1) to (7). The dimensional representation of the boundary and initial conditions[16,21,26,29] is as follows:

$$\begin{cases} \bar{w}_1 = 0, \bar{T} = \bar{T}_w, \bar{C} = \bar{C}_w, \bar{N} = \bar{N}_w & ; \bar{r}_1 = \bar{R}(\bar{z}_1) \\ \frac{\partial \bar{w}_1}{\partial \bar{r}_1} = 0, \frac{\partial \bar{T}}{\partial \bar{r}_1} = 0, \frac{\partial \bar{C}}{\partial \bar{r}_1} = 0, \frac{\partial \bar{N}}{\partial \bar{r}_1} = 0 & ; \bar{r}_1 = 0 \\ \bar{w}_1 = 0, \bar{T} = 0, \bar{C} = 0, \bar{N} = 0 & ; \bar{t}_1 = 0 \end{cases} \quad (8)$$

According to Kumar and Kumar[16] Mishra et al[22], the body acceleration and pressure gradient terms are given as $G(\bar{t}_1) = F_b cos(w_b \bar{t}_1 + \psi)$ and $-\frac{\partial \bar{p}_1}{\partial \bar{z}_1} = D_1 + D_2 cos\left(w_p \bar{t}_1\right)$. Here, D_1 is the amplitude of the steady pressure component, F_b is the body acceleration term, w_p is $2\pi f_p$, the term f_p represents the pulse frequency. The ψ delineated is the phase angle and w_b is $2\pi f_b$, furthermore f_p represents the frequency of the body acceleration with the phase angle. Finally, D_2 indicates the amplitude of the pulsatile pressure gradient.

If we put an axial electric field on the nanofluid, it will conduct electricity. The Poisson-Boltzmann equation to define the electroosmotic potential function is according to Manchi and Ponalagusamy[21] and the final solution after applying the Debye-Huckel linearization to the Poisson equation along with the specified boundary condition[22] is $\psi_1(r_1) = \frac{I_0(K_e r_1)}{I_0(K_e R)}$.

Dimensional Analysis: Transforming the model into a dimensionless format simplifies analysis, finds universal behaviors and emphasizes significant physical impacts via dimensionless parameters. By enabling predictions and comparisons across other systems, these metrics offer crucial insights into the behavior of the blood flow[2,11,21,26].

$r_1 = \frac{\bar{r}_1}{\bar{R}_0}$, $w_1 = \frac{\bar{w}_1}{\bar{U}_0}$, $u_1 = \frac{\bar{L}_1 \bar{u}_1}{\bar{\delta}_s \bar{U}_0}$, $t_1 = \frac{\bar{U}_0 \bar{t}_1}{\bar{R}_0}$, $z_1 = \frac{\bar{Z}_1}{\bar{L}_1}$, $p_1 = \frac{\bar{R}_0^{\,2} \bar{p}_1}{\bar{R}_0 \bar{U}_0 \mu_0}$, $\theta = \frac{\bar{T}-\bar{T}_1}{\bar{T}_w-\bar{T}_1}$, $\phi = \frac{\bar{C}-\bar{C}_1}{\bar{C}_w-\bar{C}_1}$, $N = \frac{\bar{N}-\bar{N}_1}{\bar{N}_w-\bar{N}_1}$, $M^2 = \frac{\sigma_f \bar{R}_0^2 B_r^2}{\mu_f}$, $R = \frac{\bar{R}}{\bar{R}_0}$, $Re = \frac{\bar{U}_0 \rho_f \bar{R}_0}{\mu_f}$, $E_1 = \frac{E_z}{B_r \bar{U}_0}$, $Gr = \frac{\gamma_f \rho_f \bar{R}_0^{\,2} g(\bar{T}_w-\bar{T}_1)}{\bar{U}_0 \mu_f}$, $Gc = \frac{\gamma_f \rho_f \bar{R}_0^{\,2} g(\bar{C}_w-\bar{C}_1)}{\bar{U}_0 \mu_f}$, $Rb = \frac{\gamma_f \rho_f \bar{R}_0^{\,2} g(\bar{N}_w-\bar{N}_1)}{\bar{U}_0 \mu_f}$, $Ec = \frac{\bar{U}_0^2}{c_f(\bar{T}_w-\bar{T}_1)}$, $Pr = \frac{\mu_f c_p}{k_f}$, $Q_0 = \frac{Q\bar{R}_0^{\,2}}{k_f(\bar{T}_w-\bar{T}_1)}$, $S_z = \frac{\bar{R}_0^{\,2} E_z^{\,2}}{k_f(\bar{T}_w-\bar{T}_1)}$, $K_e = \frac{\bar{K}_e}{\bar{R}_0}$, $Sc = \frac{\nu}{D_c}$, $Pe = \frac{b\,W_c}{D_m}$, $\sigma_1 = \frac{\bar{N}}{\bar{N}_w-\bar{N}_1}$ (9)

The non-dimensional parameters from the equation (9) are integrated into the governing equations (1) to (8). The stenosis is presumed to be mild, characterized by a maximum height significantly lower than the artery's radius $\delta_s \ll 1$ and the length of the stenotic region is proportional to the artery's radius expressed as $\varepsilon(= \bar{R}_0/\bar{L}_1) = O(1)$. The subsequent expression represents the modified governing equations (1) to (7):

Continuity equation:

$$\frac{\partial w_1}{\partial z_1} = 0 \quad (10)$$

Momentum equation:
r_1-direction

$$\frac{\partial p_1}{\partial r_1} = 0 \quad (11)$$

z_1-direction

$$\frac{\rho_{nf}}{\rho_f}\frac{\mu_f}{\mu_0} Re \frac{\partial w_1}{\partial t_1} = -\frac{\partial p_1}{\partial z_1} + \frac{1}{2}\frac{1}{\mu_0}\frac{1}{r_1}\frac{\partial}{\partial r_1}\left[\mu_{nf}(\theta) r_1 \frac{\partial w_1}{\partial r_1}\right] + \frac{(\rho\gamma)_{nf}}{(\rho\gamma)_f}\frac{\mu_f}{\mu_0}(Gr\,\theta + Gc\,\phi - Rb\,N)cos(\eta_0) + F_b cos(c_2 t_1 + \psi) + U_{hs} K_e^2 \psi_1(r_1) - \frac{\sigma_{nf}}{\sigma_f}\frac{\mu_f}{\mu_0} M^2 w_1 \quad (12)$$

Energy equation:

$$Pr\, Re \frac{k_f}{k_{nf}}\frac{(\rho c_p)_{nf}}{(\rho c_p)_f}\frac{\partial \theta}{\partial t_1} = \frac{\partial^2 \theta}{\partial r_1^2} + \frac{1}{r_1}\frac{\partial \theta}{\partial r_1} + Q_0 \frac{k_f}{k_{nf}} + \frac{k_f}{k_{nf}}\frac{\sigma_{nf}}{\sigma_f} Ec\, M^2\, Pr\, w_1^2 + \frac{k_f}{k_{nf}}\frac{\sigma_{nf}}{\sigma_f} S_z + Ec\, Pr\, \frac{k_f}{k_{nf}}\frac{\mu_{nf}}{\mu_f}\left(\frac{\partial w_1}{\partial r_1}\right)^2 \quad (13)$$

Concentration equation:

$$Re\, Sc\, \frac{\partial \phi}{\partial t_1} = \frac{\partial^2 \phi}{\partial r_1^2} + \frac{1}{r_1}\frac{\partial \phi}{\partial r_1} - k_1(1+\theta\alpha)^q exp\left(-\frac{E_n}{1+\theta\alpha}\right)\phi \quad (14)$$

Microorganisms equation:

$$Re\, Sb\, \frac{\partial N}{\partial t_1} = \frac{\partial^2 N}{\partial r_1^2} + \frac{1}{r_1}\frac{\partial N}{\partial r_1} - Pe\left[\frac{\partial N}{\partial r_1}\frac{\partial \phi}{\partial r_1} + (\sigma_1 + N)\frac{\partial^2 \phi}{\partial r_1^2}\right] \text{n} \quad (15)$$

Ellahi et al[9] demonstrated that Reynold's viscosity model accounts for temperature-dependent viscosity and pressure

gradient, body acceleration and dimensionless form of the stenosed artery by incorporating dimensionless variables into the equation (12):

$$\mu_f(\theta) = \mu_0(1-\beta_0\theta), \qquad -\frac{\partial p_1}{\partial z_1} = B_1[1 + e\,cos(c_1\,t_1)],$$
$$G(t_1) = F_b\,cos(c_2\,t_1 + \psi)$$
$$R(z_1) = \begin{cases} 1 - \delta_s\,sin\big(\pi(z_1 - d_1)\big)\,; & d_1 \le z_1 \le d_1 + 1 \\ 1 & ;\ otherwise \end{cases}$$

where, $\beta_0 \ll 1$, $e = \frac{D_2}{D_1}$, $B_1 = \frac{D_1 \bar{R}_0{}^2}{\bar{U}_0 \mu_0}$, $c_1 = \frac{2\,\pi\,\bar{R}_0\,f_p}{\bar{U}_0}$, $F_b = \frac{\bar{F}_b \bar{R}_0{}^2}{\bar{U}_0 \mu_0}$, $c_2 = \frac{\bar{R}_0\,f_b}{\bar{U}_0}$ and $t_1 > 0$

To achieve a rectangular domain, it is essential to implement the transformation $x = \frac{r_1}{R(z_1)}$ on the geometry in equations (10) to (15).

The WSS, Sherwood number, Nusselt number at the artery's wall[16, 17, 20, 21, 26] and the volumetric flow rate[17, 21, 26] are provided as follows.

$$\tau_w = -\frac{1}{R}\left(\frac{\partial w_1}{\partial x}\right)_{x=1},\ Sh = -\frac{1}{R}\left(\frac{\partial \phi}{\partial x}\right)_{x=1},\ \tau_w = -\frac{1}{R}\left(\frac{\partial \theta}{\partial x}\right)_{x=1},$$
$$Q_F = 2\pi\,R^2 \int_0^1 w_1\,x\,dx$$

A variety of established numerical techniques exist for addressing partial differential equations. The acquisition of the exact solution for the transformed non-linear partial differential equations presents significant challenges, yet it remains within the realm of possibility. Consequently, it is essential to utilize numerical techniques to obtain approximate solutions for the non-linear partial differential equations presented in the current model. Hoffmann and Chiang[12] present a comprehensive overview of the FTCS algorithm, an explicit finite-difference method adept at addressing these equations through the discretization of the partial differential equations.

Furthermore, the researchers Zaman et al[35], Tripathi et al[32], Zaman et al[34], Adak[1] and Zaman et al[33] have employed this technique in their studies. The process initiates with the discretization of the spatial domain. At each time instant t_{1_k}, the values for the velocity component w_1, temperature (θ), concentration (ϕ) and microorganism (N) are computed for each x_i, denoted as $w_1(i,k)$, $\theta(i,k)$, $\phi(i,k)$ and $N(i,k)$ respectively. The partial derivatives are characterized as

$$\frac{\partial w_1}{\partial x} \cong \frac{w_1(i+1,k) - w_1(i-1,k)}{2\,\Delta x},\quad \frac{\partial w_1}{\partial t_1} \cong \frac{w_1(i,k+1) - w_1(i,k)}{\Delta t_1},\quad \frac{\partial^2 w_1}{\partial x^2} \cong \frac{w_1(i+1,k) - 2\,w_1(i,k) + w_1(i-1,k)}{\Delta x^2}$$

To ensure the stability of the solution, the step sizes are chosen as $\Delta x = 0.025$ and $\Delta t_1 = 0.0001$[12].

Result and Discussion

The numerical outcomes are derived utilizing the FTCS numerical scheme. Table 1 and table 2 present the thermophysical characteristics and properties of nanofluid and nanoparticles respectively. These tables were compiled by Khanduri and Sharma[15], Saeed et al[24], Alghamdi et al[3], Mishra et al[22] and Al-Kouz et al[5].

Table 1
Thermophysical characteristics and properties of nanofluid

Properties	**Mathematical expression for nanofluid[3,5,15,22,24]**
Viscosity	$\mu_{nf} = \frac{\mu_f}{(1-\phi_{Au})^{2.5}}$
Density	$\rho_{nf} = \phi_{Au}\rho_{Au} + (1-\phi_{Au})\rho_f$
Heat Capacity	$(\rho c_p)_{nf} = \phi_{Au}(\rho c_p)_{Au} + (1-\phi_{Au})(\rho c_p)_f$
Thermal Conductivity	$\frac{k_{nf}}{k_f} = \frac{k_{Au} + (m-1)k_f - (m-1)\phi_{Au}(k_f - k_{Au})}{k_{Au} + (m-1)k_f + \phi_{Au}(k_f - k_{Au})}$
Electrical Conductivity	$\frac{\sigma_{nf}}{\sigma_f} = \frac{\sigma_{Au} + (m-1)\sigma_f - (m-1)\phi_{Au}(\sigma_f - \sigma_{Au})}{\sigma_{Au} + (m-1)\sigma_f + \phi_{Au}(\sigma_f - \sigma_{Au})}$
Thermal Expansion Coefficient	$(\rho\gamma)_{nf} = \phi_{Au}(\rho\gamma)_{Au} + (1-\phi_{Au})(\rho\gamma)_f$

Table 2
Thermophysical characteristics and properties of nanoparticles

Thermophysical properties	**Blood**	**Gold nanoparticle (Au)**
Density $[\rho(kg/m^3)]$	1063	19320
Heat Capacity $[c_p(J/kgK)]$	3594	129
Thermal Conductivity $[K(W/mK)]$	0.492	314
Electrical Conductivity $[\sigma(S/m)]$	0.667	4.10×10^7
Thermal Expansion Coefficient $[\gamma(K^{-1})]$	1.8×10^{-6}	1.4×10^{-5}

The likely quantities that were investigated for the various flow parameters are presented as magnetic field parameter $(0-5)$[21,22], Gr $(0-8)$[27], Gc $(0-8)$[22], Pr $(7-25)$[21,22], Rayleigh number $(0-5)$[22,27], Schmith number $(0-10)$[22,27], Joule heating parameter (0.4)[22,27], Debye-Huckel parameter $(0-1)$[22,27], Activation energy parameter $(0-10)$[22, 27], Reynolds number $(0-8)$[22], Peclet number (0.2)[27], Heat source (0.3)[22,27], Electro-osmotic parameter $(0-1)$[21,26], Casson fluid parameter $(0-1)$[8,26], along with the source of those values[8,21,22,26-29].

Tripathi et al[32] studied the consistency and validation of this research. To corroborate the numerical solution of the present analysis with the published work[32], the supplementary parameters of both the current study and the aforementioned study are presented to be zero. Validation plots are illustrated in fig. (2) and fig. (3). Fig. (2) corroborates the velocity profile results whereas fig. (3) substantiates the temperature profile results. The results unequivocally demonstrate that the findings of the present paper align very well with the validation presented by Tripathi et al[32].

Fig. 4 demonstrates the velocity profile with the pure blood, Rayleigh number and presence of nanoparticles. The solid line represented the blood velocity in the presence of gold nanoparticles, whereas the dotted line illustrated the velocity of the pure blood. Initially, as seen in fig. (4), the velocity decreased upon the introduction of the gold nanoparticle into the blood vessel (artery). The fluctuation of Rayleigh number from 0 to 1 diminishes velocity trends. Fig. (5) shows the impact of the thermal Grashof number on the velocity profile. The Gr is a quantity in fluid dynamics that quantifies the significance of buoyant forces relative to viscous forces in fluid flow such as blood. Fig. 5 illustrates three various values of the Gr ($Gr = 0, 0.5$ and 1).

As the Gr grows, the velocity profile rises due to the predominance of buoyant forces. The value of Gr is zero, indicating that the buoyancy force is insignificant. The Gr rises with an increase in temperature difference between adjacent layers or a higher thermal expansion coefficient, resulting in enhanced natural convection and subsequently elevating the velocity of blood flow in the artery. Fig. (6) shows the impact of the Gc on the velocity profile. The Gc quantifies the ratio of buoyancy force due to solute concentration gradients to viscous forces in blood flow. If the values of the Gc increase from 0 to 0.8, then the velocity profile increases. The Gc increases due to a greater solute concentration difference, then the buoyancy effect enhanced blood velocity.

A high Gc leads to increased mixing of solutes such as glucose, oxygen, or pharmaceutical drugs in the artery. The increased and dispersion are benefits of a high Gc in targeted medication administration, such as using nanoparticles. Fig. 7 demonstrates the microorganism profile. It shows the microorganism profile correlation with the bioconvection Lewis number increases. The Le is the ratio of thermal diffusion to mass diffusion in a fluid. Le increases (Le =1 to 3) leading to a dominance of thermal diffusion over mass diffusion, resulting in a reduction in microorganism profile and impacting flow dynamics in stenosed arteries. This decrease in microorganism density disrupts natural density gradients contributing to bioconvective flows.

The reduced microorganism profile impaired oxygen and nutrient transport downstream of the stenosis, potentially leading to hypoxia. Increased thermal diffusion is the cause of localized heating near the stenosis, but the lack of adequate mass diffusion prevents compensatory solute transport. The reduced microorganism activity and impaired diffusion slow the removal of waste products or toxins from the blood, contributing to worsening stenosis, A disrupted balance of heat and mass diffusion can aggravate the artery's compromised state, increasing the risk of conditions like thrombosis or ischemia. Fig. 8 illustrates the microorganism profile as an effect of the Pe. The Pe is the ratio of advective transport to diffusive transport.

The Pe is a measure of blood flow in a stenosed artery, indicating the importance of advective and diffusive transport processes. As the Pe increases from 0.5 to 1.5, advective transport becomes more significant, reducing the microorganism profile and disrupting bioconvection patterns on which microorganism rely on for their distribution across the vessel walls. Low Pe (0.5) indicate diffusion where microorganisms disperse primarily due to molecular diffusion. High Pe (1.5) indicates advective transport, where the bulk flow of blood transports microorganisms, oxygen, or nutrients.

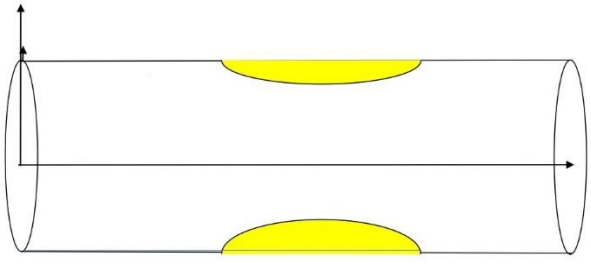

Fig. 1: Diagram of the artery

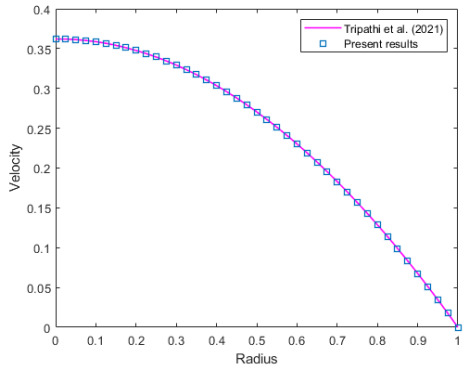

Fig. 2: Velocity profile for the pure blood for the present results[32]

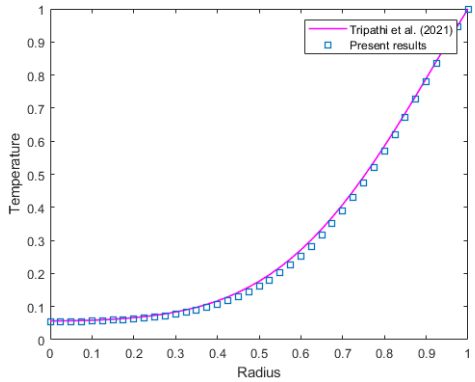

Fig. 3: Temperature profile for the pure blood for the present results[32]

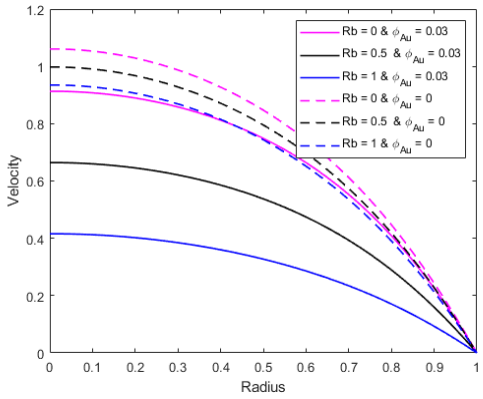

Fig. 4: Velocity profile with pure blood, Rayleigh number and presence of nanoparticle

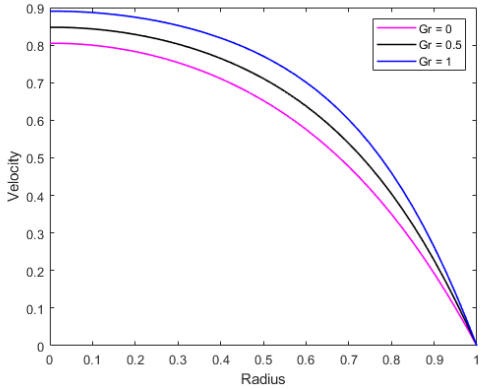

Fig. 5: Velocity profile with the presence of gold nanoparticles for various values of thermal Grashof number ($Gr = 0, 0.5$ and 1)

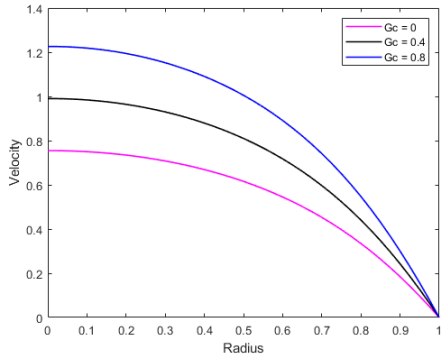

Fig. 6: Velocity profile with the presence of gold nanoparticles for various values of thermal Grashof number ($Gc = 0, 0.4$ and 0.8)

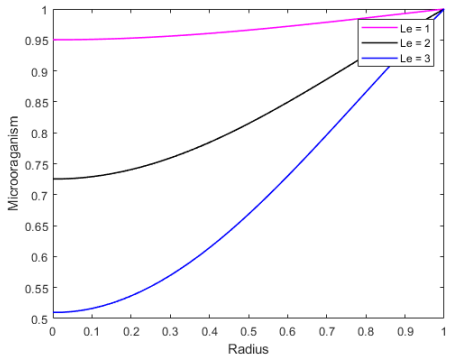

Fig. 7: Microorganism profile with the presence of gold nanoparticles for various values of bioconvective Lewis number ($Le = 1, 2$ and 3)

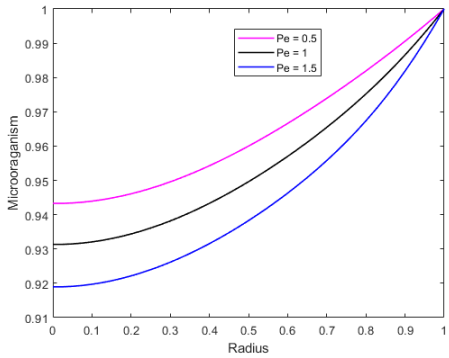

Fig. 8: Microorganism profile with the presence of gold nanoparticles for various values of Peclet number ($Pe = 0.5, 1$ and 1.5)

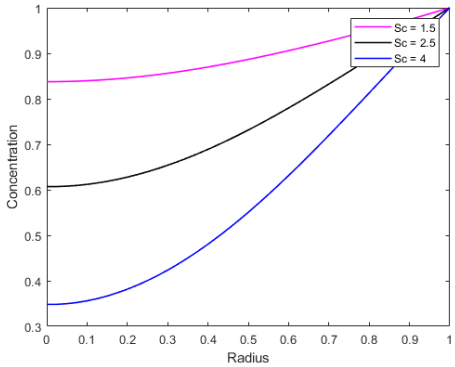

Fig. 9: Concentration profile with the presence of gold nanoparticles for various values of Schmidt number ($Sc = 1.5, 2.5$ and 4)

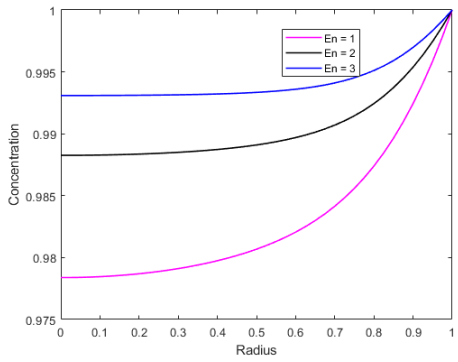

Fig. 10: Concentration profile with the presence of gold nanoparticles for various values of activation energy parameter ($En = 1, 2$ and 3)

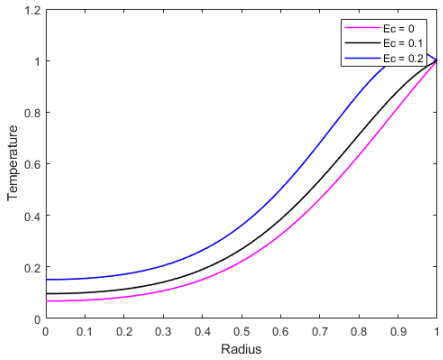

Fig. 11: Temperature profile with the presence of gold nanoparticles for various values of Eckert number ($Ec = 0, .1$ and 0.2)

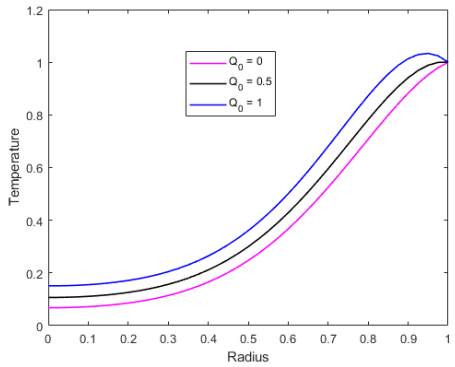

Fig. 12: Temperature profile with the presence of gold nanoparticles for various values of heat source parameter ($Q_0 = 0, 0.5$ and 1)

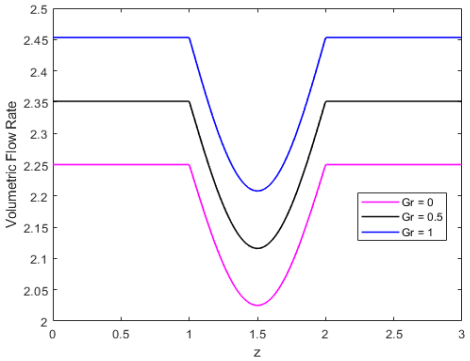

Fig. 13: Volumetric flow rate with the presence of gold nanoparticles for various values of the thermal Grashof number ($Gr = 0, 0.5$ and 1)

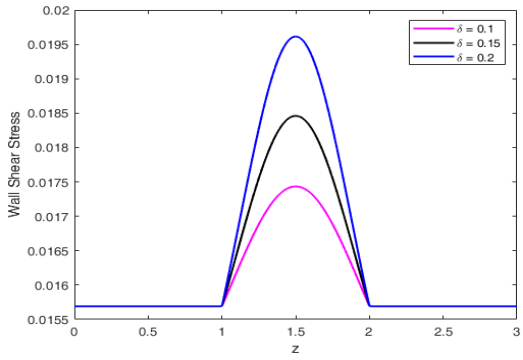

Fig. 14: Wall shear stress with the presence of gold nanoparticles for various values of depth of the stenosis ($\delta = 0.1, 0.15$ and 0.2)

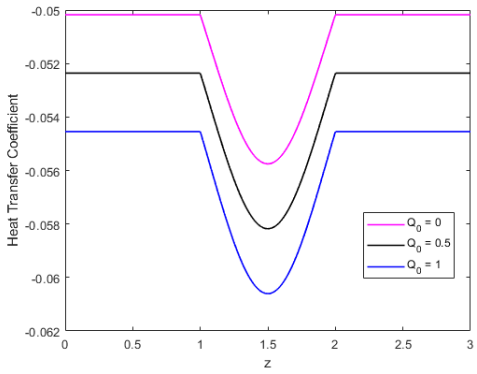

Fig. 15: Heat transfer coefficient with the presence of gold nanoparticles for various values of heat source parameter ($Q_0 = 0, 0.5$ and 1)

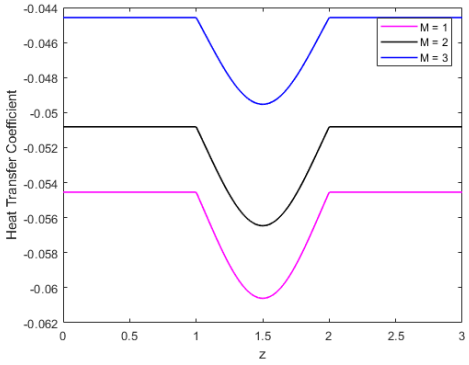

Fig. 16: Heat transfer coefficient with the presence of gold nanoparticles for various values of magnetic field parameter ($M = 1, 2$ and 3)

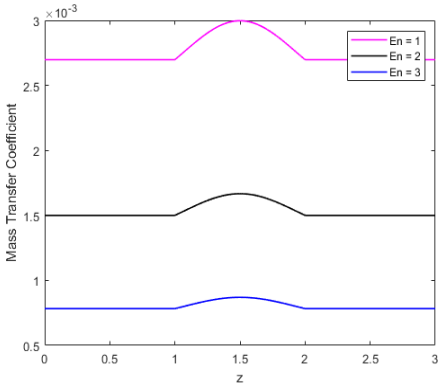

Fig. 17: Mass transfer coefficient with the presence of gold nanoparticles for various values of activation energy parameter ($En = 1, 2$ and 3)

Fig. 9 shows the concentration with variation in the Sc. he Sc is crucial to understand the relationship between momentum and mass transport in blood flow through a stenosed artery. The high Sc (4) indicates that momentum diffusion dominates, causing solutes or particles to diffuse slower than momentum transfer. Conversely, the low Sc (1.5) indicates that mass diffusion is faster than momentum diffusion, causing essential solutes to diffuse faster. This leads to a reduction in concentration in areas of low flow near the stenosis, further depleting the concentration profile. Fig. 10 displays the feature of the concentration profile under the impact of the En. The energy of activation is the minimum energy required for a chemical or physical process to occur. It is often used in transport phenomena to describe how temperature affects diffusivity or viscosity. If the values of the En increase from 1 to 3, then the concentration profile increases. The higher En for diffusion reduces solutes' ability evenly, especially in areas of low flow, like near stenosis. The temperature profile with the variation of the Ec is represented in fig. 11. The Ec is a parameter that measures the conversion of kinetic energy into heat in a fluid flow. It is particularly important in stenosed arteries where viscous effects generate significant heat. The temperature profile increases with the increase in the Ec from 0 to 0.2. A higher Ec indicates more kinetic energy is converted into thermal energy, causing a rise in blood temperature. This is particularly relevant in stenosed regions where blood accelerates due to narrow passage. The Ec directly influences temperature distribution in the artery, affecting blood viscosity, solute transport and tissue response. As the Ec increases, the conversion of kinetic energy into thermal energy becomes more pronounced, leading to localized heating. The results are notable when increases the Ec and it is helpful in biological systems like blood flow through the stenosed arteries.

Fig. 12 illustrates the temperature profile as an effect of the Q_0. The Q_0 serves as a critical dimensionless metric in fluid dynamics, particularly in biological systems such as blood flow through stenosed arteries. As the Q_0 increases from 0 to 1, the temperature profile exhibits an upward trend, clearly illustrated in the graph, indicating a nearly positive effect on the artery wall. It quantifies the rate of heat generation or absorption per unit volume, reflecting the interplay between metabolic activity, viscous dissipation and external thermal influences. This phenomenon demonstrates that the temperature profile growth is directly associated with the parameters of the heat source and noticeable results near the arterial wall. Elevated values of heat source parameters suggest substantial metabolic heat production, which is particularly relevant in pathological conditions where increased cellular activity may exacerbate.

Fig. 13 demonstrates the volumetric flow rate with the Gr. This graph indicates the volumetric flow rate accelerates when the value of the Gr increases from 0 to 1. If the Gr is low, the buoyancy forces are insignificant and the velocity field in the stenosis region is solely influenced by the pressure gradient and viscous forces. In this instance, buoyancy exerts no substantial influence on the volumetric flow rate. When a high Gr (1) is present, buoyancy forces dominate. As the Gr rises, the walls of the stenosed artery heat up and buoyancy forces facilitate the flow, resulting in localized flow acceleration and an increase in the effective volumetric flow rate. The study of wall shear stress (WSS) is crucial for understanding the complex dynamics of blood flow and pathological changes associated with conditions like stenosis. Fig. 14 illustrates the wall shear stress patterns for significant stenotic depth (δ_s). The WSS rises as the δ_s values grow, signifying an acceleration in WSS values with the escalation of stenotic depth. WSS is the tangential force per unit area applied by blood flow on the arterial wall. As the depth of the stenosis increases, the artery's cross-sectional area diminishes, resulting in an elevation of velocity. This heightened velocity amplifies the velocity gradient, thereby increasing wall shear stress. The peak WSS is observed at the most constricted segment of the stenosis, as the velocity is maximal at the momentum due to flow acceleration.

The heat transfer coefficient (Nusselt Number) quantifies the rate of convective heat transfer occurring between a fluid medium and the surface in contact with that fluid flow. Fig. 15 and fig. 16 illustrate the influence of the Q_0 and magnetic field parameter on the Nusselt number, respectively. The influence of heat source parameters on Nusselt number profiles is prominently illustrated in fig. 15. The Nusselt profile decreases as the Q_0 increases due to the production of more heat, resulting in enhanced conductive heat transfer. The influence of magnetic field parameters on the profiles of the heat transfer coefficient is illustrated in fig. 16. With a decrease in the thermal boundary layer thickness of suspensions and enhanced heat conduction facilitated by nanoscale particles, the profiles demonstrate improvement as M values increase. The mass transfer coefficient is affected by the activation energy, as seen in fig. 17. If the activation energy increases from 1 to 3, then the mass transfer coefficient profile decreases. An increase in activation energy results in diminished diffusivity, consequently yielding a reduced Sherwood number. In stenosed arteries, the influence of activation energy on flow resistance, diffusivity and mass transport is critical, as it directly affects oxygen delivery and the diffusion of drugs.

Conclusion

The graphical analyses have been provided concerning the influence of serval physical parameters, including Rayleigh number, Gr, Gc, Le, Pe, Sc, activation energy parameter, Eckert number, heat source parameter, magnetic field parameter and stenosis depth on various factors such as blood velocity, concentration, temperature, microorganisms, wall shear stress, heat transfer rate and Sherwood number. The results of this kind of analysis are highly relevant for clinical researchers and biologists, since they enable the prediction of endothelial cell damage and lipid build up in response to particular wall shear stress patterns in blood

arteries. This study presents significant findings resulting from current mathematics research.

- The increment in the thermal Grashof number leads to a rise in the velocity and volumetric flow rate while an increment in the Rayleigh number leads to decrement in the velocity profile.
- If Q is accelerated, then the blood temperature increases while the Nusselt number decreases.
- The application of Au nanoparticles have demonstrated a reduction in lipid accumulation in cardiovascular disease therapy by elevating blood temperature.
- The results demonstrate that an increase in the activation energy parameter reduces the Sherwood number and enhances the concentration.

References

1. Adak M., Comparison of explicit and implicit finite difference schemes on diffusion equation, In Bhattacharyya S., Kumar J., Ghoshal K., Mathematical Modeling and Computational Tools, ICACM 2018, Springer Proceedings in Mathematics & Statistics, Springer, Singapore, **320**, 227-238 **(2020)**

2. Ahmed S.E., Arafa A.A. and Hussein S.A., Bioconvective flow of a variable properties hybrid nanofluid over a spinning disk with Arrhenius activation energy, Soret and Dufour impacts, *Numerical Heat Transfer, Part A: Applications*, **85(6)**, 900-922 **(2024)**

3. Alghamdi W., Alsubie A., Kumam P., Saeed A. and Gul T., MHD hybrid nanofluid flow comprising the medication through a blood artery, *Scientific Reports*, **11(1)**, 11621 **(2021)**

4. Alharbi F.M., Naeem M., Zubair M., Jawad M., Jan W.U. and Jan R., Bioconvection due to gyrotactic microorganisms in couple stress hybrid nanofluid laminar mixed convection incompressible flow with magnetic nanoparticles and chemical reaction as carrier for targeted drug delivery through porous stretching sheet, *Molecules*, **26(13)**, 3954 **(2021)**

5. Al-Kouz W., Shah S.Z.H., Souayeh B., Sabir Z. and Owhaib W., A novel tetra hybrid bio-nanofluid model with stenosed artery, *Open Physics*, **22(1)**, 20240091 **(2024)**

6. Bacha H.B., Ullah N., Hamid A. and Shah N.A., A comprehensive review on nanofluids: synthesis, cutting-edge applications and future prospects, *International Journal of Thermofluids*, **22**, 100595 **(2024)**

7. Bhatti M.M., Zeeshan A. and Ellahi R., Simultaneous effects of coagulation and variable magnetic field on peristaltically induced motion of Jeffrey nanofluid containing gyrotactic microorganism, *Microvascular Research*, **110**, 32-42 **(2017)**

8. Das D., Shaw S., Mondal K.K. and Kairi R.R., Analyzing the impact of boundary slip and absorption effects on the dispersion of solute in a pulsatile channel flow of Casson fluid under magnetic field, *The European Physical Journal Plus*, **138(5)**, 372 **(2023)**

9. Ellahi R., Raza M. and Vafai K., Series solutions of non-Newtonian nanofluids with Reynolds' model and Vogel's model by means of the Homotopy analysis method, *Mathematical and Computer Modelling*, **55(7-8)**, 1876-1891 **(2012)**

10. Galley H.F. and Webster N.R., Physiology of the endothelium, *British Journal of Anaesthesia*, **93(1)**, 105-113 **(2004)**

11. Hafed Z.S., Arafa A.A., Hussein S.A., Ahmed S.E. and Morsy Z., Bioconvective blood flow of tetra composition nanofluids passing through a stenotic artery with Arrhenius energy, Numerical Heat Transfer, Part B: Fundamentals, 1-24 **(2023)**

12. Hoffmann K.A. and Chiang S.T., Computational fluid dynamics, Engineering Education System, Wichita, USA **(2000)**

13. Issacci F., Ghoniem N.M. and Catton I., Magnetohydrodynamic flow in a curved pipe, *The Physics of Fluids*, **31(1)**, 65-71 **(1988)**

14. Karmakar P. and Das S., Electro-blood circulation fusing gold and alumina nanoparticles in a diverging fatty artery, *Bio Nano Science*, **13(2)**, 541-563 **(2023)**

15. Khanduri U. and Sharma B.K., Hall and ion slip effects on hybrid nanoparticles (Au-GO/blood) flow through a catheterized stenosed artery with thrombosis, Proceedings of the Institution of Mechanical Engineers, Part C: Journal of Mechanical Engineering Science, **237(10)**, 2256-2278 **(2023)**

16. Kumar S. and Kumar S., Blood flow through an elliptical stenosed artery with the heat source and chemical reaction, *Res. J. Biotech.*, **17(12)**, 82-90 **(2022)**
17. Kumar S. and Kumar S., Blood flow with heat transfer through different geometries of stenotic arteries, *Trends in Sciences*, **20(11)**, 1-14 **(2023)**

18. Kumawat C., Sharma B.K. and Mekheimer K.S., Mathematical analysis of two-phase blood flow through a stenosed curved artery with hematocrit and temperature dependent viscosity, *Physica Scripta*, **96(12)**, 125277 **(2021)**

19. Kuznetsov A.V., Bio-thermal convection induced by two different species of microorganisms, *International Communications in Heat and Mass Transfer*, **38(5)**, 548-553 **(2011)**

20. Kuznetsov A.V., Nanofluid bioconvection in water-based suspensions containing nanoparticles and oxytactic microorganisms: oscillatory instability, *Nanoscale Research Letters*, **6**, 1-13 **(2011)**

21. Manchi R. and Ponalagusamy R., Modeling of pulsatile EMHD flow of Au-blood in an inclined porous tapered atherosclerotic vessel under periodic body acceleration, *Archive of Applied Mechanics*, **91(7)**, 3421-3447 **(2021)**

22. Mishra N.K., Sharma B.K., Sharma P., Muhammad T. and Perez L.M., Entropy generation optimization of cilia regulated MHD ternary hybrid Jeffery nanofluid with Arrhenius activation energy and induced magnetic field, *Scientific Reports*, **13(1)**, 14483 **(2023)**

23. Priyadharsini M. and Sheremet M., Numerical and sensitivity study on the heat transfer due to bioconvection on unsteady radiative MHD blood flow over a permeable artery with chemical reaction effects, *International Communications in Heat and Mass Transfer*, **147**, 106981 **(2023)**

24. Saeed A., Khan N., Gul T., Kumam W., Alghamdi W. and Kumam P., The flow of blood-based hybrid nanofluids with couple stresses by the convergent and divergent channel for the applications of drug delivery, *Molecules*, **26(21)**, 6330 **(2021)**

25. Sajid T., Jamshed W., Eid M.R., Altamirano G.C., Aslam F., Alanzi A.M. and Abd-Elmonem A., Magnetized cross tetra hybrid nanofluid passed a stenosed artery with nonuniform heat source (sink) and thermal radiation: Novel tetra hybrid Tiwari and Das nanofluid model, *Journal of Magnetism and Magnetic Materials*, **569**, 170443 **(2023)**

26. Sharma B.K., Khanduri U., Gandhi R. and Mahammad T., Entropy generation analysis of a ternary hybrid nanofluid (Au-CuO-GO/Blood) containing gyrotactic microorganisms in bifurcated artery, *International Journal of Numerical Methods for Heat and Fluid Flow*, **34(2)**, 980-1020 **(2024)**

27. Sharma B.K., Khanduri U., Mishra N.K., Albaijan I. and Perez L.M., Entropy generation optimization for the electroosmotic MHD fluid flow over the curved stenosis artery in the presence of thrombosis, *Scientific Reports*, **13(1)**, 15441 **(2023)**

28. Sharma B.K., Kumawat C. and Makunde O., Hemodynamical analysis of MHD two-phase blood flow through a curved permeable artery having variable viscosity with heat and mass transfer, *Biomechanics and Modeling in Mechanobiology*, **21(3)**, 797-825 **(2022)**

29. Sharma M.K., Sharma P.R. and Nasha V., Pulsatile blood flow through stenosed artery with axial translation, *International Journal of Biomathematics*, **8(3)**, 1550028 **(2015)**

30. Tang T.Q., Rooman M., Shah Z., Jan M.A., Vrinceanu N. and Racheriu M., Computational study and characteristics of magnetized gold-blood Oldroyd-B nanofluid flow and heat transfer in stenosis narrow arteries, *Journal of Magnetism and Magnetic Materials*, **569**, 170448 **(2023)**

31. Tang T.Q., Rooman M., Vrinceanu N., Shah Z. and Alshehri A., Blood flow of au-nanofluid using sisko model in stenotic artery with porous walls and viscous dissipation effect, *Micromachines*, **13(8)**, 1303 **(2022)**

32. Tripathi J., Vasu B., Beg O.A. and Gorla R.S.R., Unsteady hybrid nanoparticle-mediated magneto-hemodynamics and heat transfer through an overlapped stenotic artery: Biomedical drug delivery simulation, Proceedings of the Institution of Mechanical Engineers, Part H: Journal of Engineering in Medicine, **235(10)**, 1175-1196 **(2021)**

33. Zaman A., Ali N. and Ali I., Effects of nanoparticles (Cu (Copper), Silver (Ag)) and slip on unsteady blood flow through a curved stenosed channel with aneurysm, *Thermal Science and Engineering Progress*, **5**, 482-491 **(2018)**

34. Zaman A., Ali N. and Khan A.A., Computational biomedical simulations of hybrid nanoparticles on unsteady blood hemodynamics in a stenotic artery, *Mathematics and Computers in Simulation*, **169**, 117-132 **(2020)**

35. Zaman A., Ali N. and Sajid M., Numerical simulation of pulsatile flow of blood in a porous-saturated overlapping stenosed artery, *Mathematics and Computers in Simulation*, **134**, 1-16 **(2017)**.

(Received 05th March 2025, accepted 09th May 2025)